Electronic Supplementary Material (ESI) for Journal of Materials Chemistry A.

Support Information for:

Coaxial α-MnSe@N-Doped Carbon Double Nanotubes as Superior Anode Material in Li/Na-Ion Half/Full Batteries

Dai-Huo Liu,[ab] *Wen-Hao Li,*[a] *Hao-Jie Liang,*[a] *Hong-Yan Lü,*[a] *Jiawei Wang,*[c] *Jin-Zhi Guo,*[a] *and Xing-Long Wu**[ade]

[a] National & Local United Engineering Laboratory for Power Batteries, and Faculty of Chemistry, Northeast Normal University, Changchun 130024, China. Email addresses: xinglong@nenu.edu.cn.
[b] Collaborative Innovation Center of Henan Province for Green Manufacturing of Fine Chemicals, Key Laboratory of Green Chemical Media and Reactions, Ministry of Education, School of Chemistry and Chemical Engineering, Henan Normal University, Xinxiang 453007, Henan, P.R. China.
[c] State Key Laboratory of Electroanalytical Chemistry, Changchun Institute of Applied Chemistry, Chinese Academy of Sciences, Changchun 130022, Jilin, P.R. China.
[d] Key Laboratory for UV Light-Emitting Materials and Technology, Northeast Normal University, Ministry of Education, Changchun, Jilin 130024, P. R. China
[e] Institute of Advanced Electrochemical Energy, Xi'an University of Technology, Xi'an 710048, P. R. China.
* The corresponding author, email: xinglong@nenu.edu.cn.

The supplementary materials include:

1. Structural characterizations for the template and intermediate

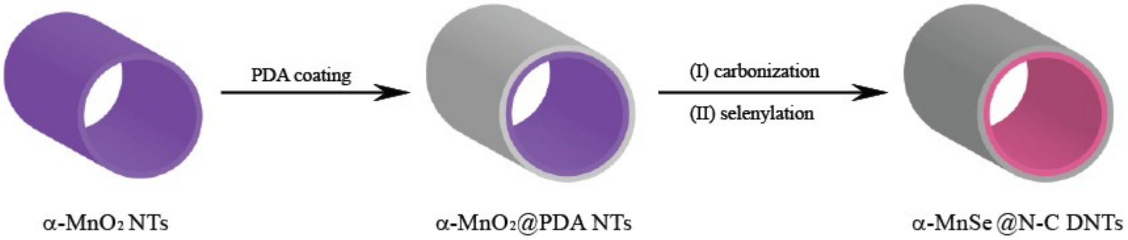

Scheme S1. Schematic of the preparation processes of the designed coaxial α-MnSe@N-C DNTs

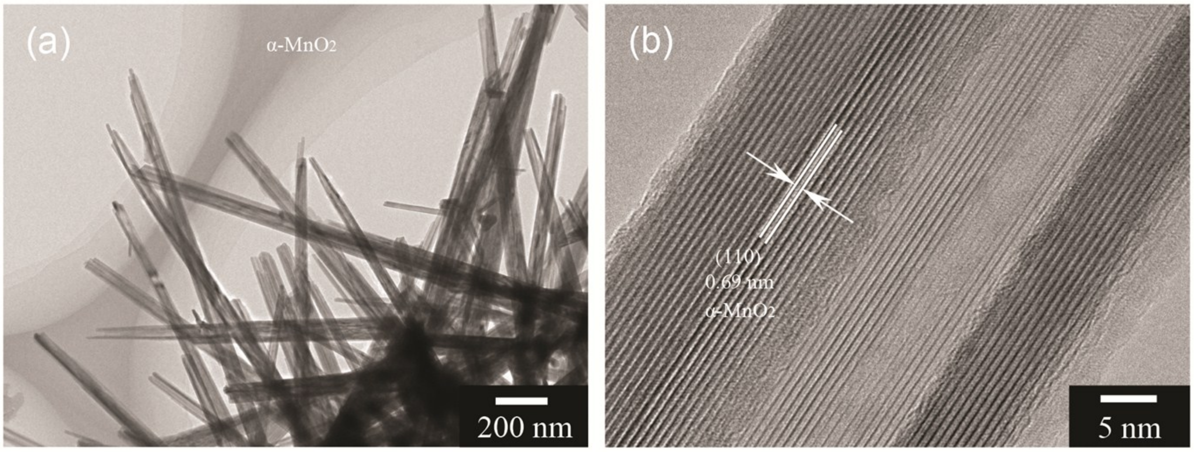

Figure S1. (a) TEM and (b) HRTEM images of α-MnO_2 NTs template.

Figure S1 shows that we successfully prepared the hollow α-MnO_2 NTs template. The hollow α-MnO_2 NTs is a typical nanotube with the dimeter of ~55 nm (55±25 nm) (Figure S1a). Figure S1b shows a HRTEM image of hollow α-MnO_2 NTs. The (110) crystal plane with lattice spacing of 0.69 nm can be observed from the α-MnO_2, which are in well agreement with XRD (Figure S4).

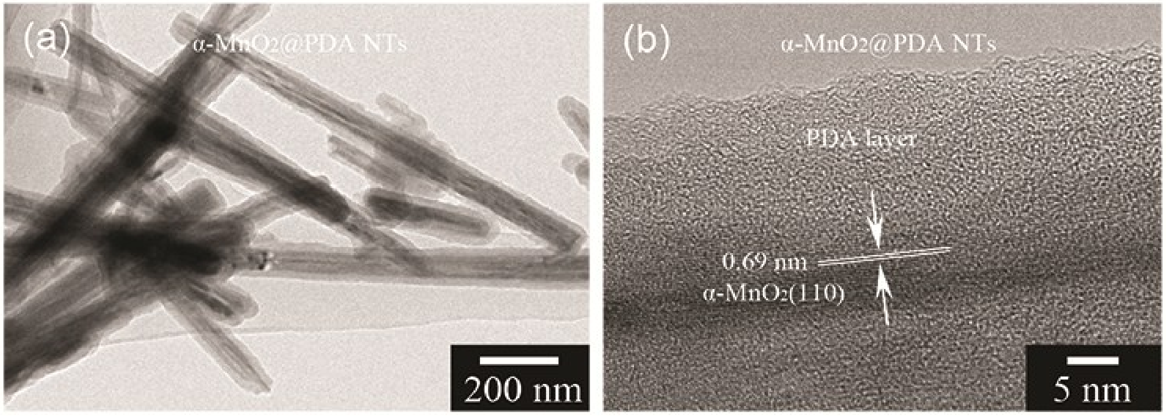

Figure S2. (a) TEM and (b) HRTEM images of α-MnO_2@PDA NTs.

Figure S2 shows that the hollow α-MnO_2 NTs template is PDA-coated successfully. The HRTEM image of coaxial α-MnO_2@PDA NTs shows that the lattice spacing of 0.69 nm corresponds to the (110) crystal plane of α-MnO_2 (Figure S2b).

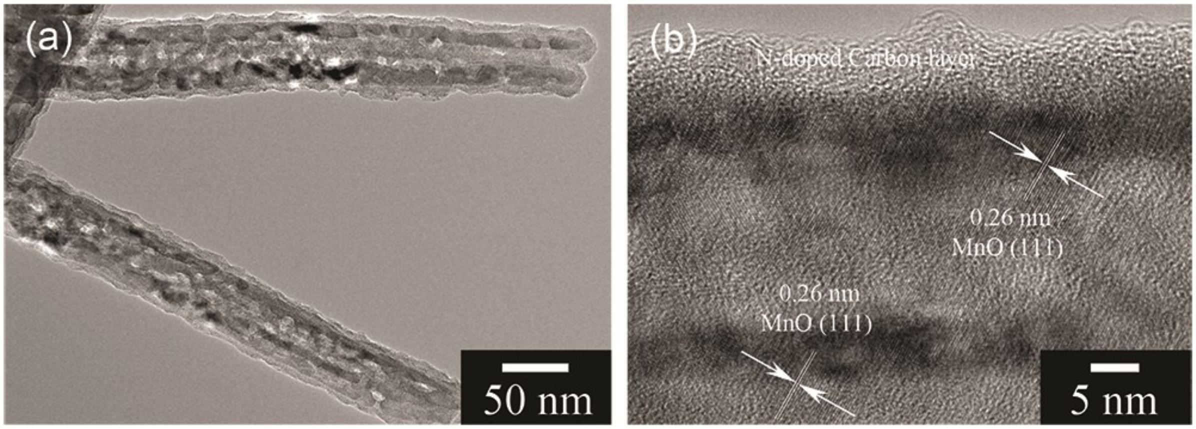

Figure S3. (a) TEM and (b) HRTEM images of MnO@N-C NTs intermediate.

Figure S3 indicates that the hollow α-MnO_2 NTs in α-MnO_2@PDA NTs precursor are reduced to MnO after carbonization, the PDA coating layer converted into amorphous N-doped carbon nanotubes (N-C NTs). The high resolution TEM image shows that the marked lattice spacing of 0.26 nm corresponds to the (111) crystal plane of MnO (Figure S3b), which agree with XRD (Figure S4).

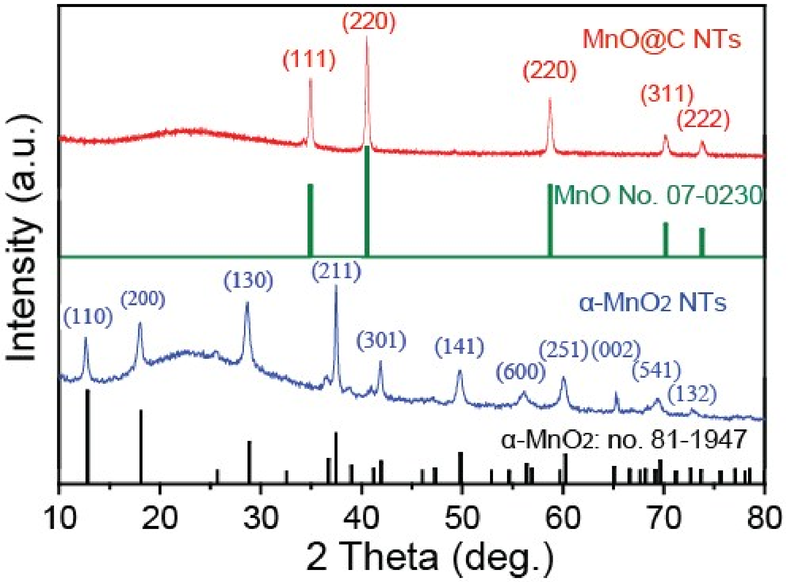

Figure S4. XRD patterns of hollow α-MnO_2 NTs template and the intermediate MnO@N-C NTs.

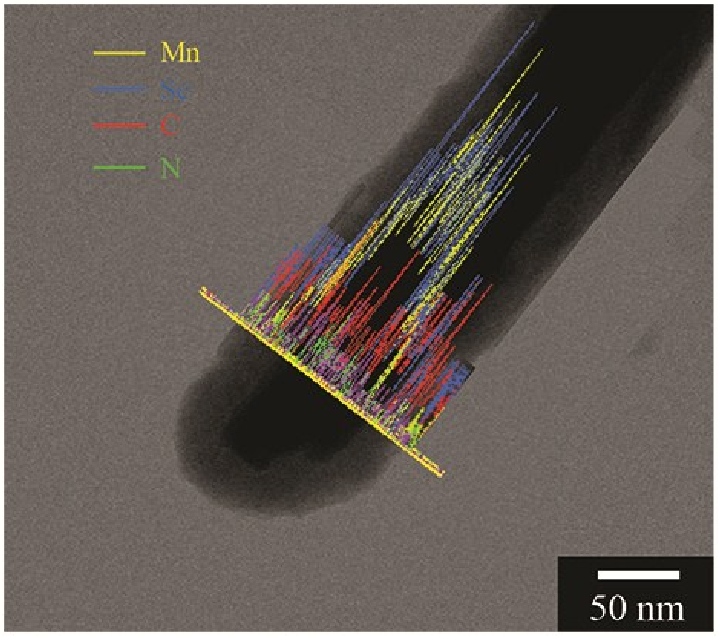

Figure S5. The line-scan TEM-EDS analysis of coaxial α-MnSe@N-C DNTs.

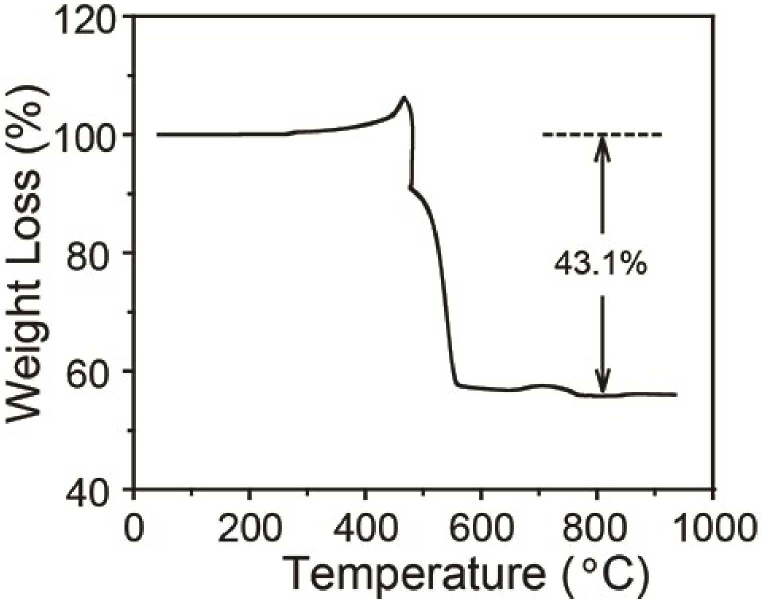

Figure S6. TGA curve of the α-MnSe@N-C DNTs tested in air. Combined with the inductively coupled plasma atomic emission spectroscopy (ICP-AES) analysis, the contents of MnSe and N-C NTs are 64.6 % and 35.4 %, respectively, in the α-MnSe@N-C DNTs.

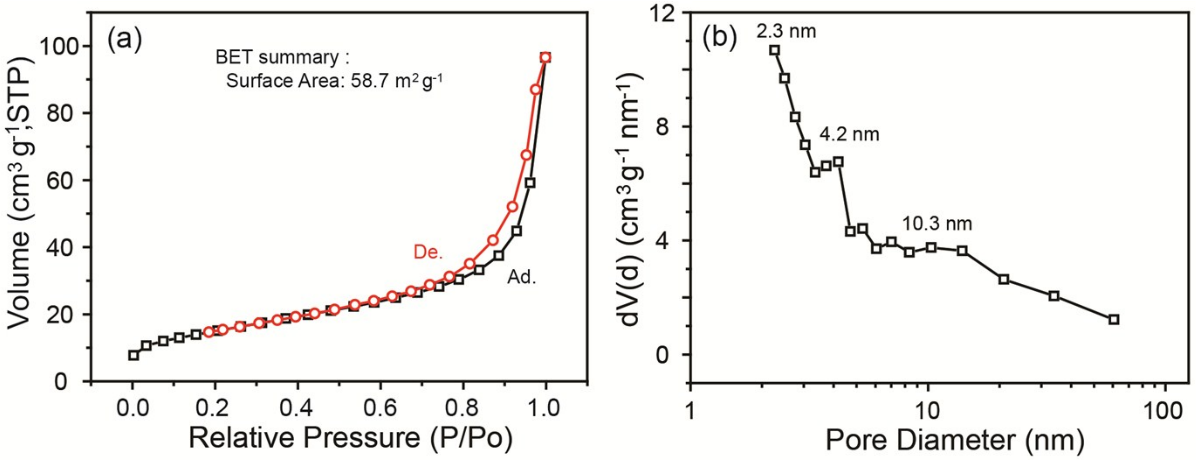

Figure S7. (a) N_2 adsorption-desorption isotherm and (b) the corresponding pore size distribution fitted from the BJH method of the prepared α-MnSe@N-C DNTs.

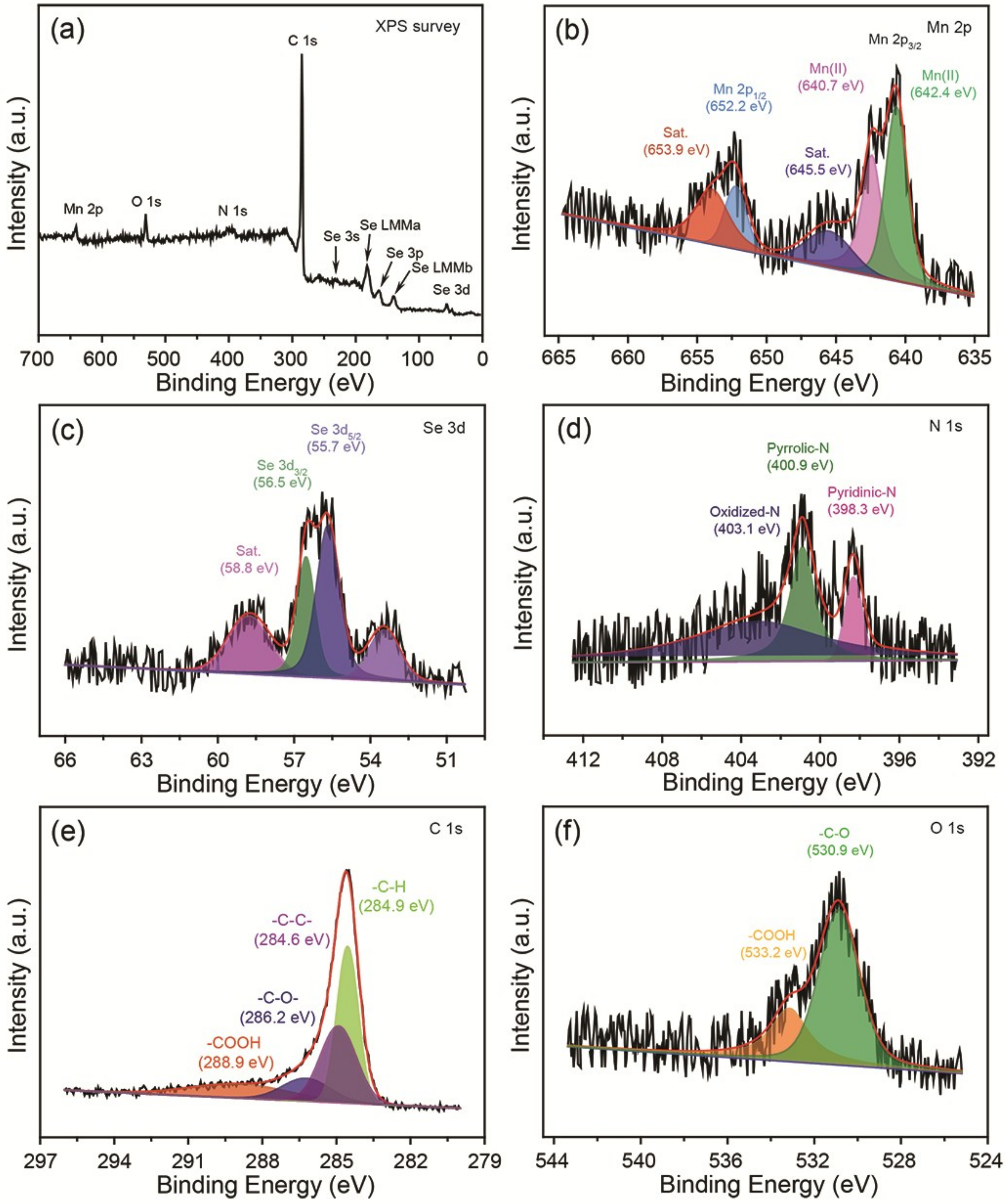

Figure S8. XPS spectra for the as-prepared α-MnSe@N-C DNTs: (a) the survey spectrum and high-resolution (b) Mn 2p, (c) Se 3d, (d) N 1s, (e) C 1s and (f) O 1s spectra.

As shown in Figure S8, the surface composition of α-MnSe@N-C DNTs and chemical states of Mn and Se were analyzed by using X-ray photoelectron spectroscopy (XPS). The overall spectrum shows the existence of Mn, Se, N, C and O (Figure S8a). While Mn 2p spectrum is composed of Mn(Ⅱ) and satellite peaks, the binding energies of Mn $2p_{3/2}$ and Mn $2p_{1/2}$ peaks were located at 642.2 and 652.2 eV, respectively (Figure S8b).[16] Figure S7c shows the high resolution XPS spectrum of Se 3d. The two peaks at 53.6 eV and 55.7 eV correspond to the binding energies of Se $3d_{5/2}$ and Se $3d_{3/2}$, respectively.[16, 23, 25, 33] The peaks at 56.5 eV and the broad peak at 58.8 eV were assigned to selenium-oxygen bonding structures at the surface.[5, 21] Three peaks centered at 398.3, 400.9 and 403.1 eV can be assigned as pyridinic-N, pyrrolic-N and oxidized-N, respectively.[32] The doped-carbon incorporated nanocomposites of such N atoms in the carbonaceous lattice will provide more electronic sites to accelerate the kinetics during the Li^+/Na^+-diffusion.[17, 22, 27, 29] The asymmetrical patterns of high-resolution C1s and O1s spectra disclose that the existence of different oxygen containing groups covalently bonded with carbon atoms.

2. Li-storage properties of the α-MnSe@N-C DNTs electrode

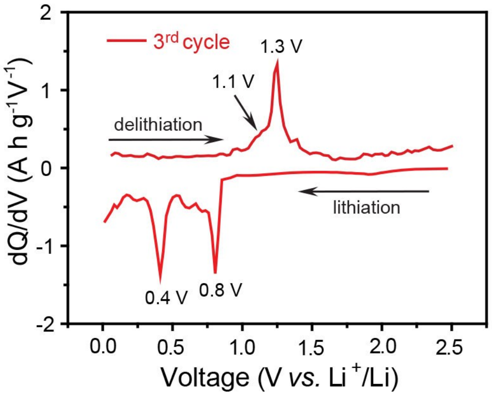

Figure S9. The dQ/dV curve of the 3rd GDC cycle of the α-MnSe@N-C DNTs electrode in Li-ion half cells.

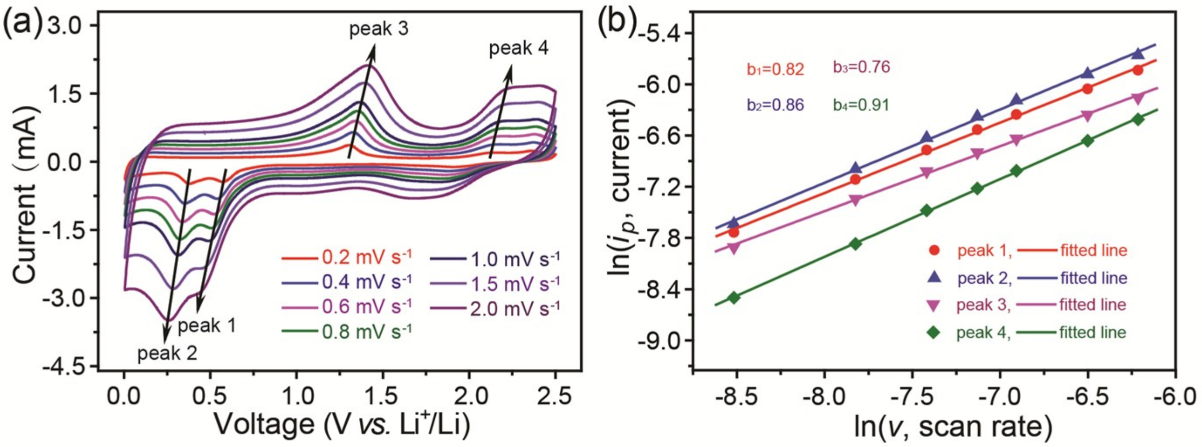

Figure S10. (a) CV curves at different scan rates from 0.2 mV s^{-1} to 2.0 mV s^{-1} and (b) corresponding $\ln(i_p)$ versus $\ln(v)$ plots at each redox peak (i_p: peak current; v: scan rate) of the α-MnSe@N-C DNTs electrode.

Figure S10b exhibits the $\ln(i_p)$ versus $\ln(v)$ curves at the two pairs of reduction and oxidation peaks according to i and v have a linear relationship as the subsequent equations 1 and 2:[1]

$$i = av^b \tag{1}$$

$$\ln(i) = b\ln(v) + \ln(a) \tag{2}$$

Where i is the peak current, v is potential sweep rate, a and b are adjustable parameters. When the value of b is close to 1, the electrochemical reaction is dominated by pseudocapacitance. Here, the b-values of peak 1, 2, 3 and 4 are 0.82, 0.86, 0.76 and 0.91, respectively, indicating the redox processes of α-MnS@N,S-NTC include partial pseudocapacitive behaviors. It is responsible for the fast Li^+ intercalation/extraction and long cyclic stability at a high current density. According to the typical classification of faradaic mechanisms (including underpotential deposition, redox pseudocapacitance and intercalation pseudocapacitance),[1, 3] the present pseudocapacitive contribution should be redox pseudocapacitance, which is concomitantly occurred with the conversion reaction between MnSe and Li (a faradaic charge-transfer process), because of the nonoccurrence of the obvious intercalation reaction and underpotential deposition.

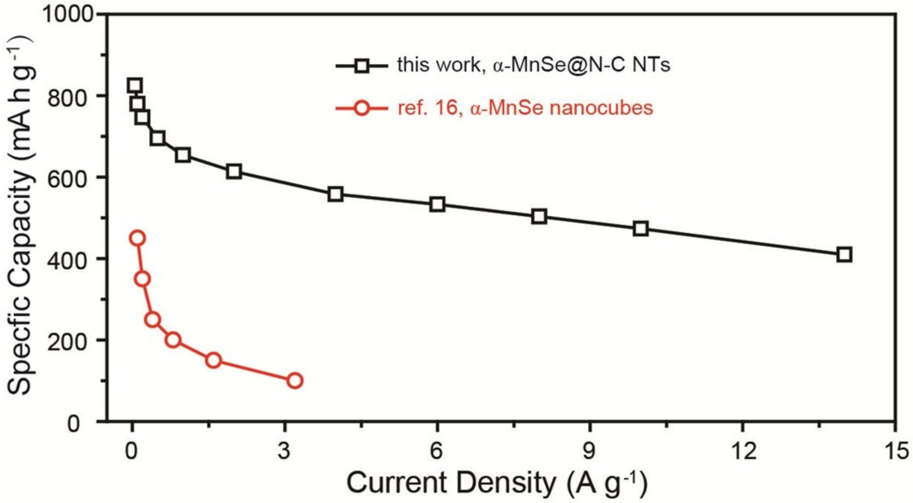

Figure S11. The comparisons of rate capability for Li-storage performance between α-MnSe@N-C DNTs and the other MnSe-based composite reported previously[16].

Table S1. Cycling performance of α-MnSe@N-C DNTs and other various chalcogenides based electrodes in LIBs.[4, 8-11, 14, 15, 18, 19, 26, 28, 30, 31, 34-36]

Morphology of materials	**Voltage Range (V *vs.* Li^+/Li)**	**Cycles (times)**	**Current density (A g^{-1})**	**C_s (mA h g^{-1})**	**Reference**
$Co_{0.85}Se$ nanosheets	0.01-3	50	0.5	300	34
$MoSe_2$/RGO	0.01-3	1000	1	600	19
In_3Se_4 nano/microstructures	0.01-3	38	0.05	600	8
CNTs@C@Bi_2Se_3	0.01-3	300	1	260	11
$Cu_{2-x}Se$@C@$MoSe_2$	0.01-3	300	1	180	10
NiS nanoplates	0.005-3	100	1	500	4
$NiSe_2$ nanoplates	0.005-3	100	1	280	4
Sb_2Se_3 nanowire	0.01-3	50	0.1	490	18
Hierarchical MoS_2 microboxes	0.05-3	50	0.1	860	30
SnS_2 nanoparticles/N-doped graphene sheets	0.01-3	100	0.1	1380	9
Single-layered MoS_2 assembled nanotubes	0.01-3	50	0.1	900	35
MoS_2 nanosheets on N-doped carbon nanoboxes	0.005-3	200	0.4	952	26
CuS/Graphene Composite	1.0-3	1000	2	360	28
NiS_2@CoS_2 hetero-nanocrystals composite	0.01-3	100	1	670	15
FeS nanodots	1.0-3	50	0.3	400	36
Co-Zn-S@N-S-C-CNT	0.005-3	100	0.1	900	14
MnS microboxes	0.01-3	100	0.2	495	31
Coaxial α-MnSe@N-C DNTs	**0.005-2.5**	**9000**	**2**	**492**	**this work**

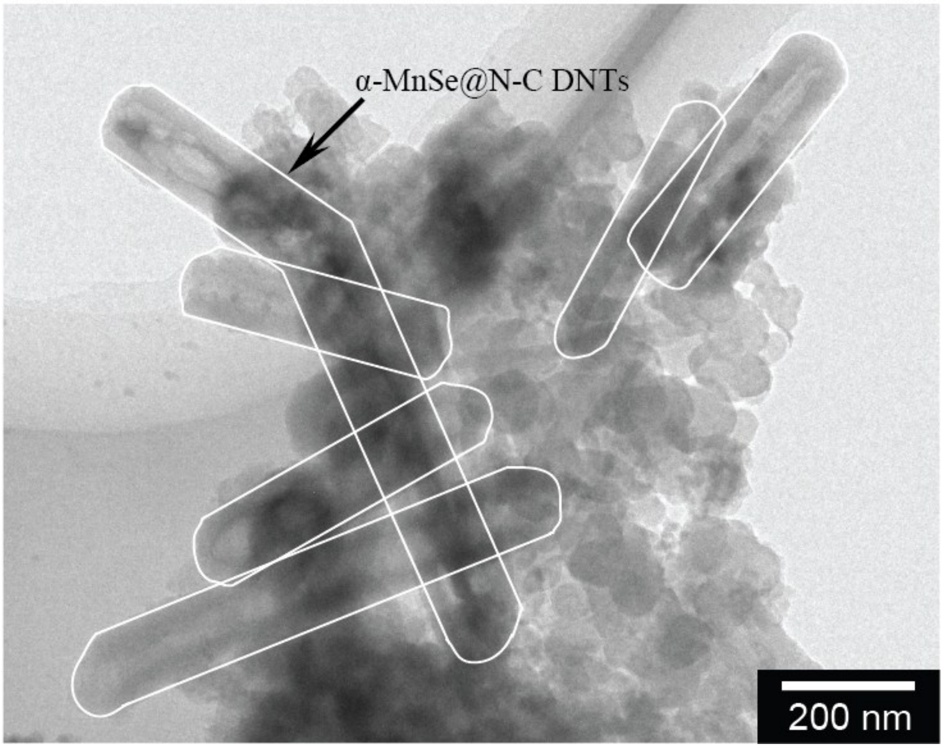

Figure S12. TEM image of α-MnSe@N-C DNTs in LIBs after 1000 cycles.

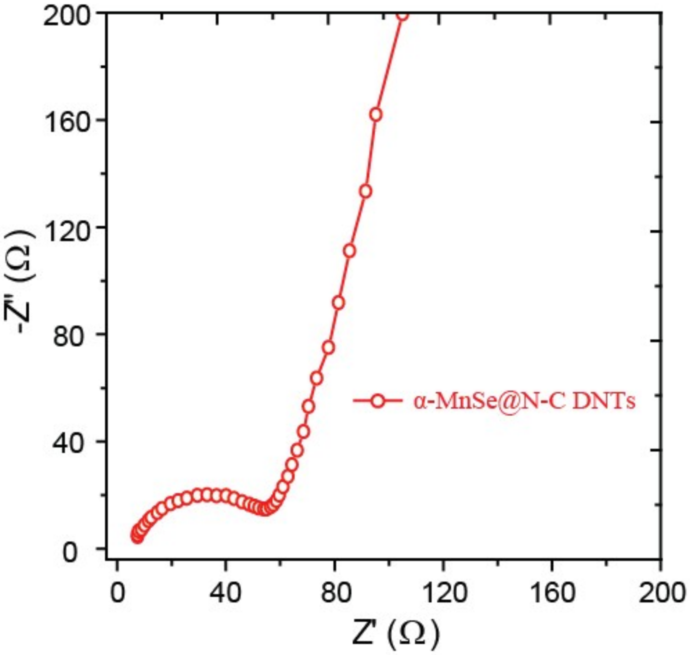

Figure S13. The Nyquist EIS plots of the α-MnSe@N-C DNTs electrode in LIBs.

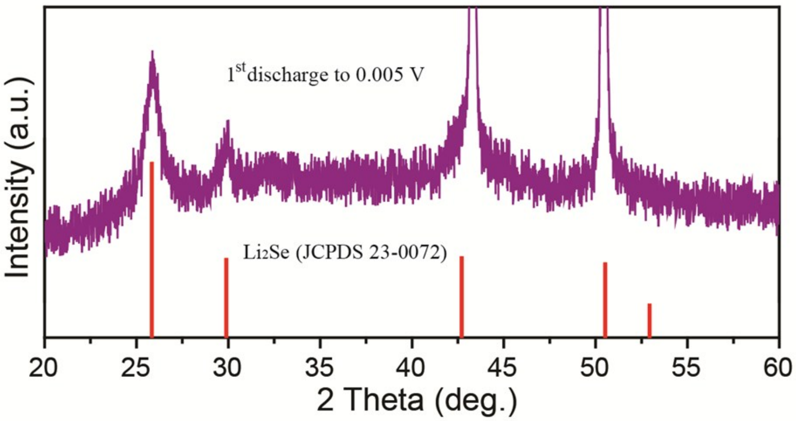

Figure S14. *Ex situ* XRD pattern of the α-MnSe@N-C DNTs electrode at the 1st discharge to 0.005 V in LIBs.

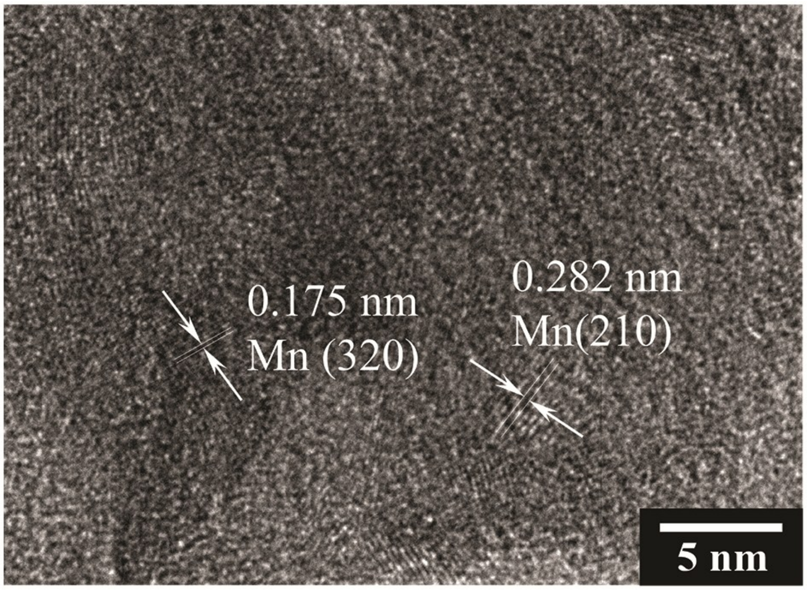

Figure S15. *Ex situ* HRTEM image of α-MnSe@N-C DNTs electrode at the 1st discharge to 0.005 V in LIBs.

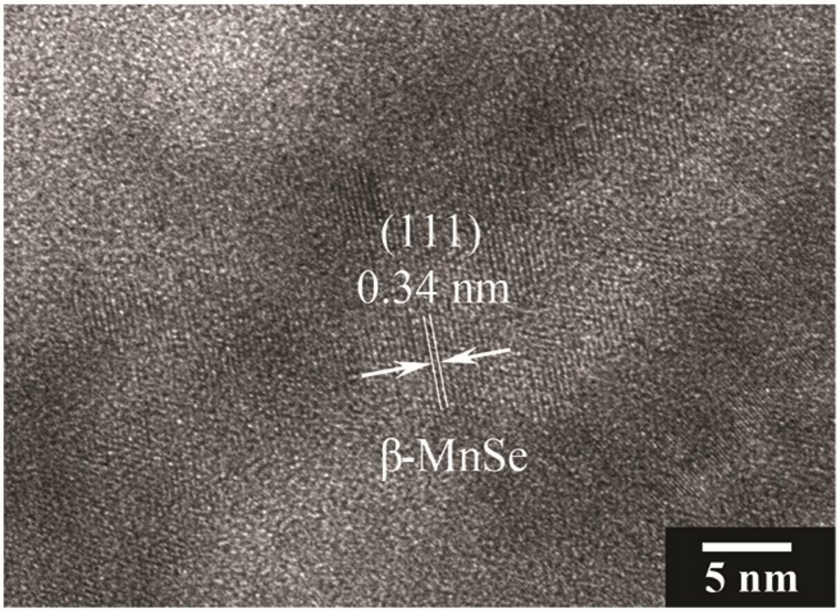

Figure S16. *Ex situ* HRTEM image of α-MnSe@N-C DNTs electrode after 200 cycles in LIBs.

Table S2. The values of electrical resistivity (ρ) and conductivity (σ) of α-MnSe@N-C DNTs, and the three contrasts of N-C NTs (α-MnSe removed), pure α-MnSe and PDA NTs.

Materials	PDA	bulk α-MnSe	α-MnSe@N-C DNTs	N-C NTs
ρ (Ω · m)	53.30	2.75	2.6×10^{-1}	2.49×10^{-1}
σ (S · m^{-1})	1.88×10^{-2}	3.64×10^{-1}	3.85	4.02

It is shown from Table S2 that, the electrical conductivities of PDA NTs and N-C NTs are 1.88×10^{-2} and 4.02 S m^{-1}, respectively. Obviously, the electrical conductivity of carbonaceous material increase over two orders of magnitude after carbonization, demonstrating that the high conductivity can be achieved by carbonizing the polydopamine at 450 °C although the formed carbonaceous material is not graphitized well. In addition, the N-C NTs significantly increase the conductivity of α-MnSe from 3.64×10^{-1} S m^{-1} to 3.85 S m^{-1} of the prepared α-MnSe@N-C DNTs anode composite by self-template constructing coaxial 1D nanotube.

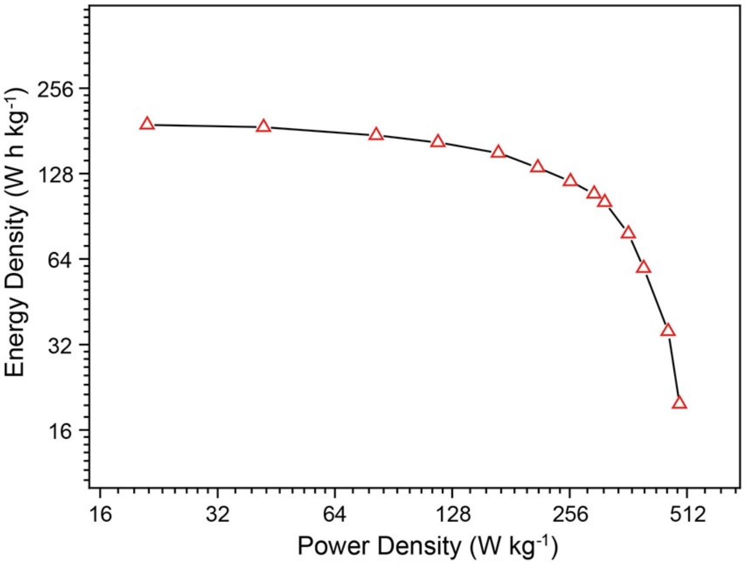

Figure S17. The Ragone plot of MSN//LFP full cell.

3. Energy-storage performance of the MSN//NCM Li-ion full cells

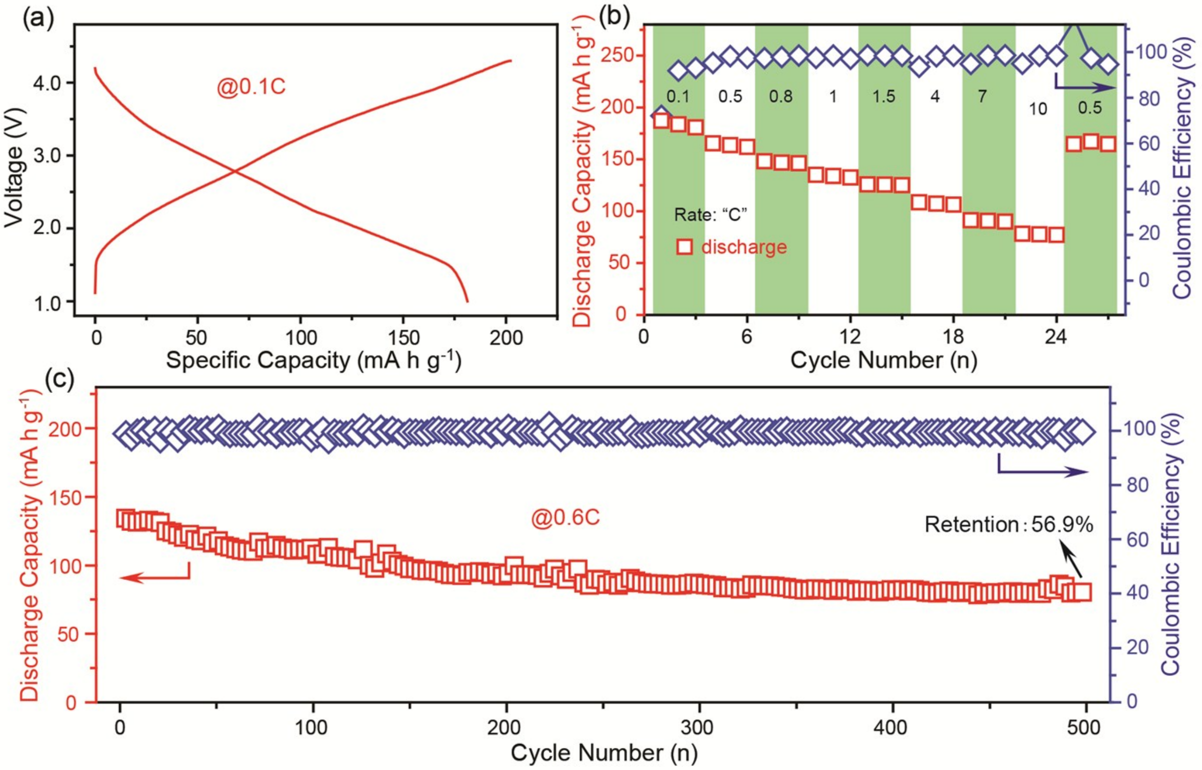

Figure S18. Energy-storage performance of the fabricated MSN//NCM full cells cycled at 1.0-4.3 V: (a) the GDC profile, (b) rate performance at various rates from 0.C to 10C, and (c) cycling performance at 0.6C.

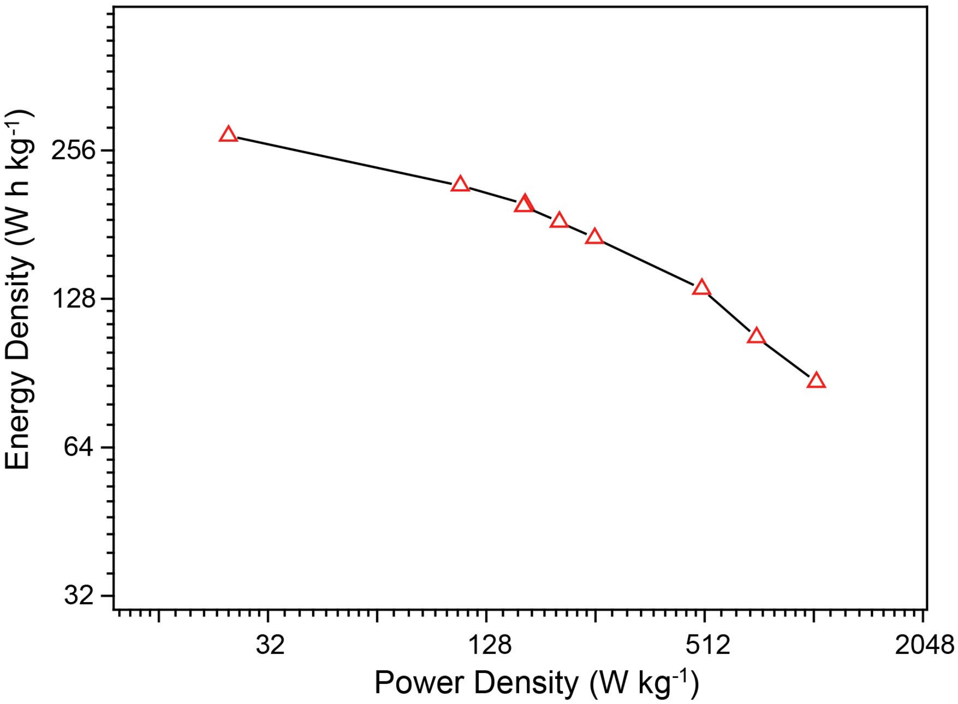

Figure S19. The Ragone plot of MSN//NCM full cell.

4. Na-storage properties of the α-MnSe@N-C DNTs electrode

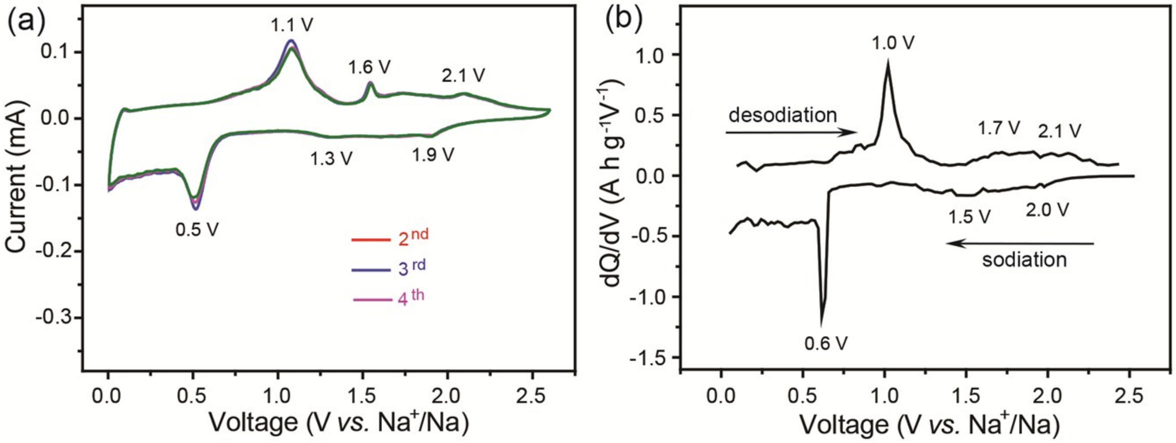

Figure S20. (a) The initial CV curves and (b) dQ/dV curve of the 3rd GDC cycle of the α-MnSe@N-C DNTs electrode in Na-ion half cells.

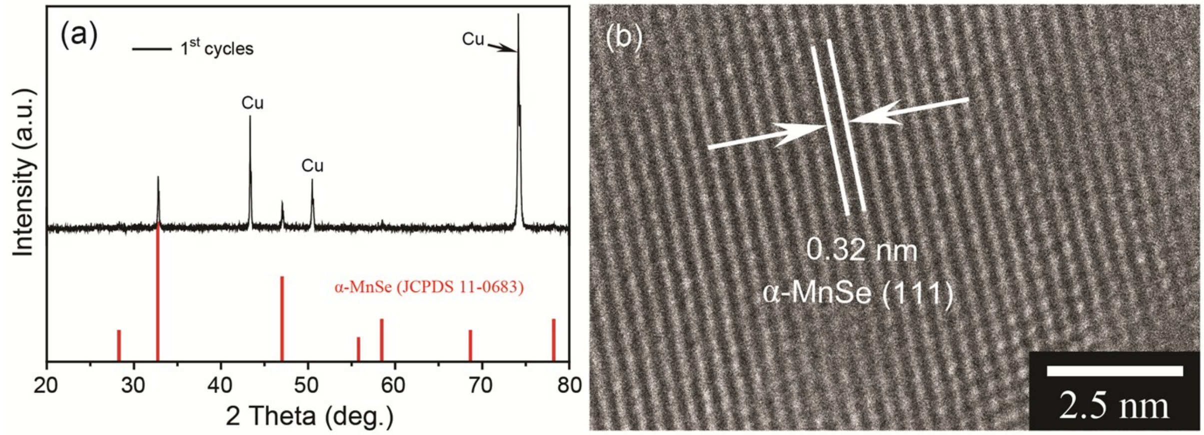

Figure S21. (a) *Ex situ* XRD pattern and (b) HRTEM image of α-MnSe@N-C DNTs electrodes at the delithiation after 1st cycle in NIBs, both of which show the presence of α-MnSe material rather than β-MnSe in the electrodes.

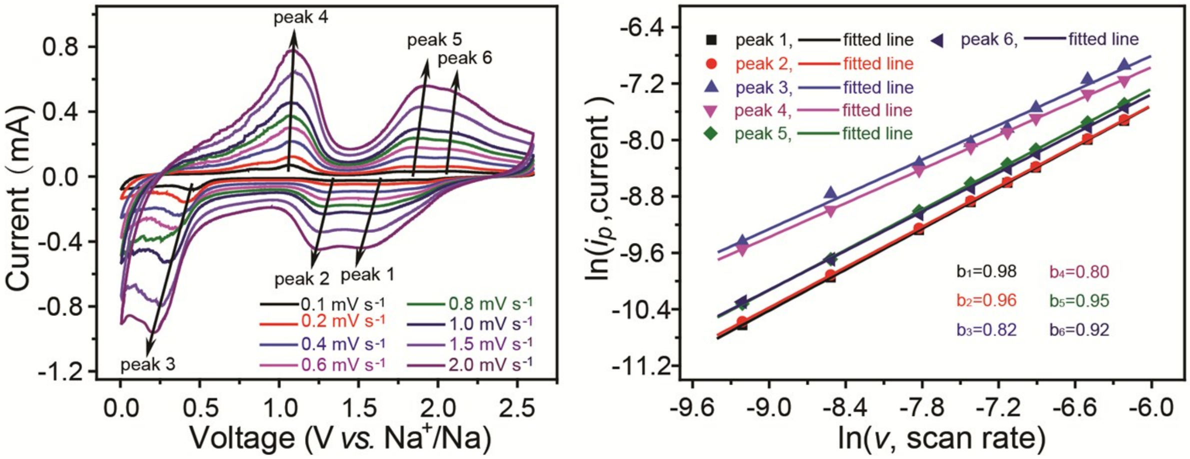

Figure S22. (a) CV curves at different scan rates and (b) corresponding ln(i_p) versus ln(v) plots at each redox peak (i_p: peak current; v: scan rate) of the α-MnSe@N-C DNTs electrode in Na-ion half cells.

5. Energy-storage performance of the MSN//NVPOF Na-ion full cells

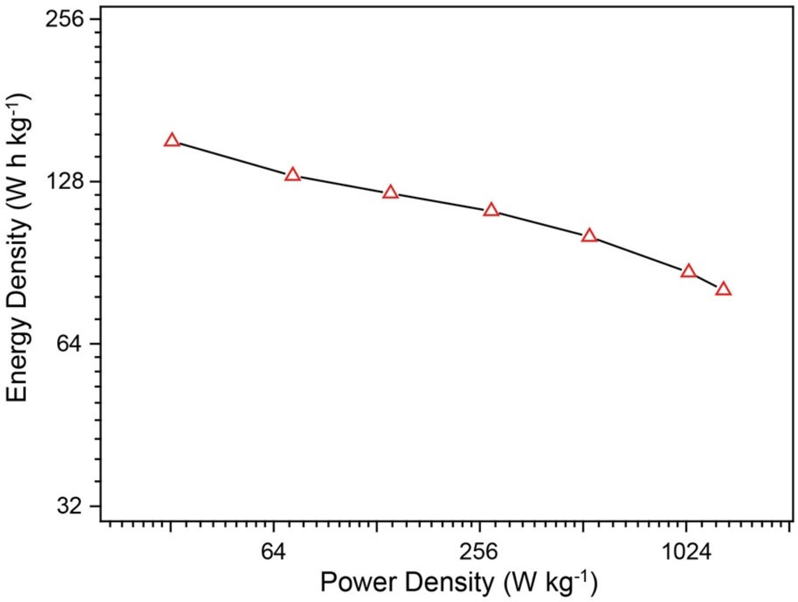

Figure S23. The Ragone plot of MSN//NVPOF full cell.

Table S3. The comparison of Na-storage performance of Na-ion full cells between the fabricated MSN//NVPOF and previously reported ones.[2, 6, 7, 12, 13, 20, 24]

Full cell (anode//cathode)	Voltage Range (V)	Cycles (times)	Rate	C_s after cycles (mA h g^{-1})	Capacity Retention	Reference
$Na_2Ti_3O_7$//$VOPO_4$	1.8-3.8	100	1C	90	92%	13
Wood carbon//$Na_3V_2(PO_4)_3$	2.0-4.3	350	0.5C	76	92%	24
Cu_3P//$Na_3V_2(PO_4)_3$	2.0-4.0	200	0.6 A g^{-1}	80	38%	6
Graphene//$Na_3V_2(PO_4)_3$	0.7-3.7	200	0.1 A g^{-1}	84	77%	2
$NaTi_2(PO_4)_3$// $Na_3V_2O_{2x}(PO_4)_2F_{3-2x}$	1.0-1.8	400	10C	30	75%	12
Zn//$Na_3V_2O_{2x}(PO_4)_2F_{3-2x}$	1.0-2.0	400	1C	46	85%	12
$NaV_{2.91}Mn_{0.09}(PO_4)_3$// $Na_3V_2(PO_4)_3$	0.5-2.5	300	5C	58	90%	20
$NaTi_2(PO_4)_3$//$Na_3V_2(PO_4)_3$	0.7-2.4	500	5C	66	67%	7
MSN//NVPOF	**1.0-4.0**	**600**	**1C**	**90**	92%	**this work**

6. References

1 T. Brezesinski, J. Wang, S.H. Tolbert, and B. Dunn, *Nat. Mater.,* 2010*,* **9**, 146-151.

2 X. Cao, A. Pan, S. Liu, J. Zhou, S. Li, G. Cao, J. Liu, and S. Liang, *Adv. Energy Mater.,* 2017*,* **7**, 1700797.

3 B.E. Conway, *Electrochemical Supercapacitors: Scientific Fundamentals and Technological Applications,* **Kluwer Academic**, 1999.

4 H. Fan, H. Yu, X. Wu, Y. Zhang, Z. Luo, H. Wang, Y. Guo, S. Madhavi, and Q. Yan, *ACS Appl. Mater. Interfaces,* 2016*,* **8**, 25261-25267.

5 H. Fan, H. Yu, Y. Zhang, J. Guo, Z. Wang, H. Wang, N. Zhao, Y. Zheng, C. Du, Z. Dai, Q. Yan, and J. Xu, *Energy Storage Mater.,* 2018*,* **10**, 48-55.

6 M. Fan, Y. Chen, Y. Xie, T. Yang, X. Shen, N. Xu, H. Yu, and C. Yan, *Adv. Funct. Mater.,* 2016*,* **26**, 5019-5027.

7 D. Guo, J. Qin, Z. Yin, J. Bai, Y.-K. Sun, and M. Cao, *Nano Energy,* 2018*,* **45**, 136-147.

8 G. Han, Z.-G. Chen, D. Ye, B. Wang, L. Yang, Y. Zou, L. Wang, J. Drennanc, and J. Zou, *J. Mater. Chem. A,* 2015*,* **3**, 7560-7567.

9 Y. Jiang, Y. Feng, B. Xi, S. Kai, K. Mi, J. Feng, J. Zhang, and S. Xiong, *J. Mater. Chem. A,* 2016*,* **4**, 10719-10726.

10 R. Jin, X. Liu, L. Yang, G. Li, and S. Gao, *Electrochim. Acta,* 2018*,* **259**, 841-849.

11 R. Jin, M. Sun, and G. Li, *Ceram. Int.,* 2017*,* **43**, 17093-17099.

12 P.R. Kumar, Y.H. Jung, C.H. Lim, and D.K. Kim, *J. Mater. Chem. A,* 2015*,* **3**, 6271-6275.

13 H. Li, L. Peng, Y. Zhu, D. Chen, X. Zhang, and G. Yu, *Energy Environ. Sci.,* 2016*,* **9**, 3399-3405.

14 H. Li, Y. Su, W. Sun, and Y. Wang, *Adv. Funct. Mater.,* 2016*,* **26**, 8345-8353.

15 H. Li, Y. Wang, J. Huang, Y. Zhang, and J. Zhao, *Electrochim. Acta,* 2017*,* **225**, 443-451.

16 N. Li, Y. Zhang, H. Zhao, Z. Liu, X. Zhang, and Y. Du, *Inorg. Chem.,* 2016*,* **55**, 2765-2770.

17 J. Liu, M. Gu, L. Ouyang, H. Wang, L. Yang, and M. Zhu, *ACS Appl. Mater. Interfaces,* 2016*,* **8**, 8502-8510.

18 W. Luo, A. Calas, C. Tang, F. Li, L. Zhou, and L. Mai, *ACS Appl. Mater. Interfaces,* 2016*,* **8**, 35219-35226.

19 Z. Luo, J. Zhou, L. Wang, G. Fang, A. Pan, and S. Liang, *J. Mater. Chem. A,* 2016*,* **4**, 15302-15308.

20 X. Ou, X. Liang, C. Yang, H. Dai, F. Zheng, P. Wu, Q. Pan, X. Xiong, and M. Liu, *Energy Storage Mater.,* 2018*,* **12**, 153-160.

21 G.D. Park, J.H. Kim, and Y.C. Kang, *Mater. Charact.,* 2016*,* **120**, 349-356.

22 L. Qie, W.M. Chen, Z.H. Wang, Q.G. Shao, X. Li, L.X. Yuan, X.L. Hu, W.X. Zhang, and Y.H. Huang, *Adv. Mater.,* 2012*,* **24**, 2047-2050.

23 T. Qin, J. Lu, S. Wei, P. Qi, Y. Peng, Z. Yang, and Y. Qian, *Inorg. Chem.Commun.,* 2002*,* **5**, 369-371.

24 F. Shen, W. Luo, J. Dai, Y. Yao, M. Zhu, E. Hitz, Y. Tang, Y. Chen, V.L. Sprenkle, X. Li, and L. Hu, *Adv. Energy Mater.,* 2016*,* **6**, 1600377.

25 Y. Tang, Z. Zhao, Y. Wang, Y. Dong, Y. Liu, X. Wang, and J. Qiu, *ACS Appl. Mater. Interfaces,* 2016*,* **8**, 32324-32332.

26 P.P. Wang, H. Sun, Y. Ji, W. Li, and X. Wang, *Adv. Mater.,* 2014*,* **26**, 964-969.

27 X. Wang, Z. Zhang, Y. Qu, Y. Lai, and J. Li, *J. Power Sources,* 2014*,* **256**, 361-368.

28 X.Y. Yu, H. Hu, Y. Wang, H. Chen, and X.W. Lou, *Angew. Chem. Int. Ed.,* 2015*,* **54**, 7395-7398.

29 C. Zhang, L. Fu, N. Liu, M. Liu, Y. Wang, and Z. Liu, *Adv. Mater.,* 2011*,* **23**, 1020-1024.

30 L. Zhang, H.B. Wu, Y. Yan, X. Wang, and X.W.D. Lou, *Energy Environ. Sci.,* 2014*,* **7**, 3302-3306.

31 L. Zhang, L. Zhou, H.B. Wu, R. Xu, and X.W. Lou, *Angew. Chem. Int. Ed.,* 2012*,* **51**, 7267-70.

32 Y. Zhang, A. Pan, L. Ding, Z. Zhou, Y. Wang, S. Niu, S. Liang, and G. Cao, *ACS Appl. Mater. Interfaces,* 2017*,* **9**, 3624-3633.

33 W. Zhao, C. Guo, and C.M. Li, *J. Mater. Chem. A,* 2017*,* **5**, 19195-19202.

34 J. Zhou, Y. Wang, J. Zhang, T. Chen, H. Song, and H.Y. Yang, *Nanoscale,* 2016*,* **8**, 14992-5000.

35 Y. Zhou, D. Yan, H. Xu, J. Feng, X. Jiang, J. Yue, J. Yang, and Y. Qian, *Nano Energy,* 2015*,* **12**, 528-537.

36 C. Zhu, Y. Wen, P.A. van Aken, J. Maier, and Y. Yu, *Adv. Funct. Mater.,* 2015*,* **25**, 2335-2342.